UNDERSTANDING THE ROLE OF MULTI-WALLED CARBON NANOTUBES IN MULTI-SCALE POROUS ULTRA-HIGH TEMPERATURE CERAMICS

Sydney Hulse and Carolina Tallon
Department of Materials Science and Engineering
Advanced Manufacturing Team
Virginia Polytechnic Institute and State University
Blacksburg, VA 24061

Abstract

Ultra-high temperature ceramics (UHTCs) are part of the thermal protection systems (TPS) of hypersonic vehicles. However, mechanical improvements are required to make effective components for commercialized hypersonics. Multi-walled carbon nanotubes (MWCNTs) have been shown to improve the mechanical properties in porous UHTCs in certain concentrations, which is predicted to be caused by phase changes. MWCNTs were incorporated in a 15vol% solid colloidal ZrB_2 suspension and slip cast before being pressureless sintered at 2000°C in vacuum and argon environment. Increases in MWCNTs concentrations for characterization was found limited to 10wt% in ZrB_2 suspensions. Comparisons between 0wt%, 10wt%, and 100wt% MWCNTs via SEM demonstrated morphological changes of green and sintered MWCNTs structures at 10wt% and 100wt% MWCNTs, but no conclusive phase changes were shown through EDS mapping. XRD of 0wt%, 10wt%, and 100wt% MWCNT in both green and sintered states showed no definitive inclusion of the MWCNTs within green or sintered states of the 10wt% MWCNT, or any indication of a phase change between materials after sintering. XPS showed no ZrC or B_4C as isothermal ternary phase diagrams at 1900°C and 2160°C have suggested. Continual investigation into the C-C bonding and MWCNTs potential phase and morphology changes are necessary.

Introduction

With the development of hypersonic vehicles, material innovations to improve thermal protection systems (TPS) have been a crucial step in commercialization. Hypersonics undergo extreme environments and must maintain mechanical integrity through sustained flight if commercialization is to be attained[1]. Extreme heat loads during flight make the distribution and peak heat flux flow a priority for the thermal protection systems. High thermal gradients exist across the vehicle as the nose and leading edges of the TPS are subjected to ranges of temperature of -170°C to 3000°C within a few centimeters[2].

Ultra-high temperature ceramics (UHTCs) offer a class of materials suitable to withstand the extreme environments with melting temperatures above 3000°C[2]. UHTCs are primarily comprised of carbides, nitrides, and borides of transition elements in group IV and V. The TPS materials are selected based upon criteria of thermal conductivities, high temperature strength, heat capacity, and oxidation resistance at high temperatures. UHTCs have become known for their tailorable microstructures through advanced manufacturing practices[2].

The addition of porosity has been shown to improve UHTCs thermal shock resistance as well as decrease thermal expansion mismatch between materials across the hypersonic vehicle[2]. Increases in porosity also show a decrease in thermal conductivity, slowing the transfer of heat across the material.

Introducing porosity in some components is also helpful in decreasing the overall mass of the structure.

The primary goal of the thermal protection system is to provide suitable durability under extreme heat fluxes, but it also needs to withstand the extreme mechanical loading happening through flight, and especially at reentry[1]. With increases in porosity, the fracture toughness of UHTCs decreases. The creation of a composite ceramic matrix has been shown to compensate for the effect of porosity on fracture toughness. In carbon-carbon (C/C) composite TPS structures with carbon nanotubes (CNTs), there are multi-scale reinforcement mechanisms at a microscopic length scale[2]. The fiber-matrix interface improved fracture toughness through grain refinement, allowance of debonding, deformation, crack deflection, and fiber pull out between the ceramic and nanoscale additive. However, while similar research in the addition of CNTs has been done on porous UHTCs, theories about strengthening mechanisms have proven inconclusive[4]. Dense ZrB_2 matrixes have seen similar CNT pull out or crack deflection and bridging as the C/C composites[3,4]. However, with a 10vol% of multi-walled carbon nanotubes (MWCNTs), the aqueous hetero-coagulated ZrB_2 matrix was shown to have unzipped graphite nanoribbons caused during spark plasma sintering[5]. Research exploring the effect of MWCNTs in UHTC bulk powder processing has not yet been successful.

MWCNTs are hexagonally bonded carbon atoms that are cylindrically layered sheets inside one another. With a high tensile strength of 63 GPa and extremely high elastic modulus of approximately 1 TPa, MWCNTs offer a promising reinforcing additive for UHTC ceramics[4]. A primary concern in working with high concentrations of MWCNTs is homogeneity of dispersion throughout the ceramic matrix[6]. Without uniform dispersion, the CNTs act as a weaker fracture point rather than strengthening the matrix. CNTs were shown to inhibit UHTC grain growth when processed at high temperatures, resulting in similar strengthening mechanisms found in the C/C composites. However, high temperatures during sintering may initiate degradation of the CNT structure[7].

Low concentrations of MWCNTs additives were introduced into ZrB_2 with control over composition and sonication parameters to facilitate uniform dispersion via colloidal processing[8]. This method was used to replica cast a multi-scale, highly porous structure. However, the identification of strengthening mechanisms was limited due to low concentrations of MWCNTs.

The work of this research will investigate the role of MWCNTs in a ZrB_2 matrix through colloidal processing. This research aids NASA's Aeronautics Research Mission Directive which outlines innovation of high-speed commercial flight, air mobility, and improvements of efficiency and safety. Hypersonics is a field of commercialization for high-speed travel and further development of thermal protection systems is required to reach long-term sustainability of these vehicles.

Procedure

Sample Preparation

C150P Baytube MWCNTs and ZrB_2 received from Höganäs were the two powders used. The ZrB_2 powder, grade B, has a particle dv_{50} = 2.3 µm. The MWCNTs have a mean outer diameter of 13 nm with an inner mean diameter of 4 nm, at a length of >1 µm and purity of >95wt%. Concentrations of 0-10wt% MWCNTs were used.

Colloidal suspensions were prepared in concentrations of 15vol% total solids in cyclohexane from Sigma Aldrich as the solvent. Commercial Hypermer A70 by Croda was used as the dispersant to prevent agglomeration of particles. Once solvent and dispersant were mixed, the MWCNTs were added in the allotted amounts and sonicated for 2 minutes at 40% power. The ZrB_2 ceramic powder was then mixed in and sonicated for 3 minutes at 40% power. The sonicated suspension was then ball-milled with tungsten carbide rolling media for 2 hours for homogenization.

Suspensions were poured into molds mounted on Plaster of Paris slabs and greased with Krytox commercial lubricant. Suspensions were then slip cast and left for 48 hours before being demolded.

An RDWebb Red Devil vacuum graphite furnace was used to sinter the MWCNT-ZrB_2 samples. The process occurs under vacuum until 1800°C where argon gas is backfilled. The maximum temperature was 2000°C and held for an hour, at ramp rates of 5°C/minute.

Characterization

i. Archimedes' Method

The Archimedes' method was used to determine density of green and sintered samples of MWCNT and ZrB_2.

ii. Scanning Electron Microscopy (SEM) and Energy-Dispersive X-ray Spectroscopy (EDS)

A JCM-7000 Benchtop Scanning Electron Microscope by JEOL was used to evaluate microstructure and elemental analysis of internal structures of green and sintered samples, with particular focus on morphology.

iii. X-Ray Diffraction (XRD)

The PANalytic Empyrean X-ray Diffractometer was used to scan at 45 kV voltage and 40 mA current. Scans were completed in 0.0131° steps with a 4.0 second sample rotation from 10° to 90° 2θ to identify different phases with the introduction of MWCNT into ZrB_2.

iv. X-ray Photoelectron Spectroscopy (XPS)

A PHI Quantera X-ray Photoelectron Spectrometer was used with an excitation source of monochromatic Al Kα. A source energy of 1486.6 eV and strength of 25 W were used with a low energy electron and argon gas flood with an electron take-off angle of 45°. The overall survey scan was at a pass energy of 280 eV at 1.0 eV steps for a total dwell time of 400 ms while the specific region scans were completed at a pass energy of 26 eV and 0.1 eV steps for a 1600 ms dwell time.

Results & Discussion

Increasing MWCNT content in samples

Prior investigation demonstrated limitations on suspension dispersion when adding additional MWCNTs into ZrB_2 via colloidal processing, with 2wt% MWCNTs being most suitable for pourable and flowable suspensions[8]. Increasing concentrations of MWCNTs in ZrB_2 were tested, from 0wt%, 3wt%, 5wt%, 8wt%, and 10wt% MWCNTs. 10wt% MWCNTs was identified as the limit amount to be used in the 15vol% due to the increased difficulty in sonication to properly de-agglomerate the MWCNTs prior to addition of ZrB_2 powder.

Phase Change Analysis

While the sintering occurs at 2000°C, there are no recorded ternary phase diagrams at this temperature so 1900°C and 2160° isothermal ternary phase diagrams of Figure 1a and 1b were found for the system of interest (Zr, B and C). The temperatures are above and below the sintering temperature used in this study. The working composition described of 10wt% MWCNTs in ZrB_2 has been identified in Figure 1 as a blue dot and green dot on 1900° and 2160°C respectively. At 1900°, the expected phases for 10wt% MWCNTs are ZrB_2, B_4C, and C phases[9]. At 2160°C, the expected phases for 10wt% MWCNTs include ZrB_2, B_4C, and C as well, but it is located near a region of just ZrB_2 and C phases[10]. In both ternary phase diagrams, the solidus line introducing a ZrC phase is near the 10wt% MWCNTs composition and could be introduced as an additional possible phase after sintering. Primary expected phases would still be B_4C alongside the ZrB_2 particles and C from MWCNTs.

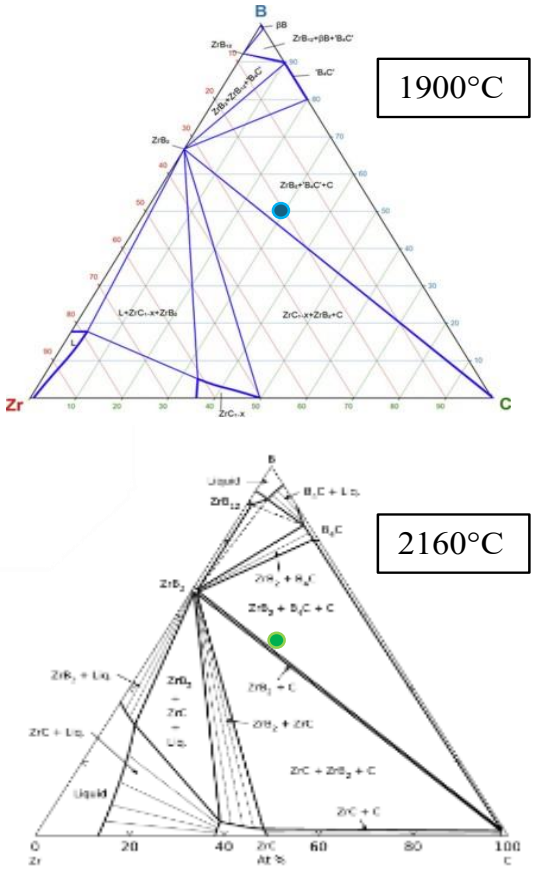

Figure 1. *The ternary phase diagram of zirconium, boron, and carbon at isothermal levels 1900°C* ***(a)***[9] *and 2160°C* ***(b)***[10] *for predicted phases.*

Microstructural analysis

Microstructure of samples containing 0wt%, 10wt%, and 100wt% MWCNTs were examined using SEM and EDS. While the MWCNTs were sonicated during suspension preparation for deagglomeration, the increasing composition of MWCNTs created larger and larger agglomerations. Unevenly distributed pockets of MWCNTs existed in high quantities across the 10wt% MWCNTs. Figure 2a and 2d show 0wt% MWCNTs green body and sintered body, and ZrB_2 particles and grain growth typically achieved during the sintering process. The sintered MWCNTs saw a change in morphology. Figure 2c shows the green MWCNTs agglomerations with more jagged edges where MWCNTs jut out from the "cloud" edges. However, after sintering, the MWCNTs seem to be more condensed, with limited MWCNTs jutting out from the cloud. The sintered clouds show visible MWCNTs branching inside the agglomerations which create a more consolidated microstructure.

EDS analysis has limited capabilities to differentiate between boron and carbon signatures. The zirconium and carbon EDS signals shown in Figure 3 depict ZrB_2 particles existing in the MWCNTs clouds with distinct boundaries. However, any distinguishing features of boron being contained in the ZrB_2 particles in the green state are absent. The boron and carbon signatures show little change in location

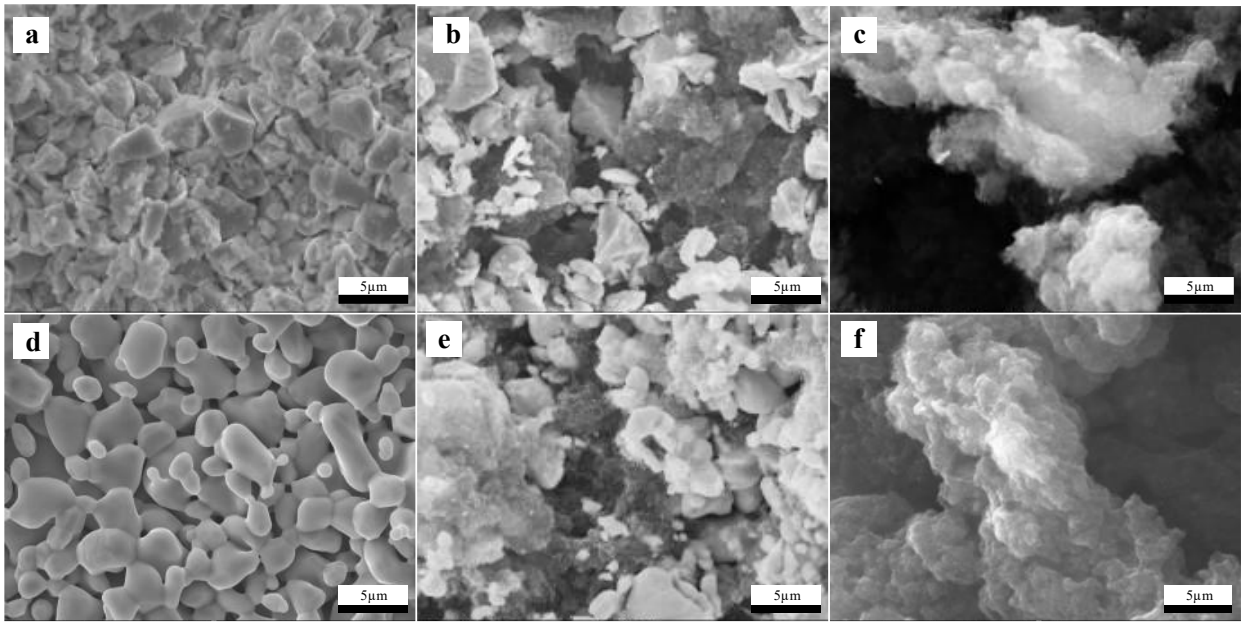

Figure 3. *SEM images of 0wt% MWCNTs green* ***(a)*** *and sintered* ***(d),*** *10wt% MWCNTs green* ***(b)*** *and sintered* ***(e)****, 100wt% MWCNTs green* ***(c)*** *and sintered* ***(f).***

compared to one another from green to sintered bodies across the 10wt% MWCNTs sample.

Phase evolution

XRD results shown in Figure 4 demonstrate no differences in phase location between the 0wt% and 10wt% MWCNTs samples. The 100wt% MWCNTs showed peaks at the same 2θ, but with greater peak widths, which is expected due to the small size of the nanotubes in comparison to the ZrB_2 particles. The overlap of peaks in both ZrB_2 and MWCNTs at 26° 2θ and around 42-43° 2θ make it difficult to differentiate which two phases are present within the green 10wt% MWCNTs, and prevent identification in the sintered 10wt% MWCNTs as well. The increase in peak width could be attributed to the MWCNTs through crystallite size or the microstrain introduced into the structure. Additional work is required to find anything definitive as there is a lack of evidence of phase changes within the ZrB_2-MWCNTs matrix post-sintering.

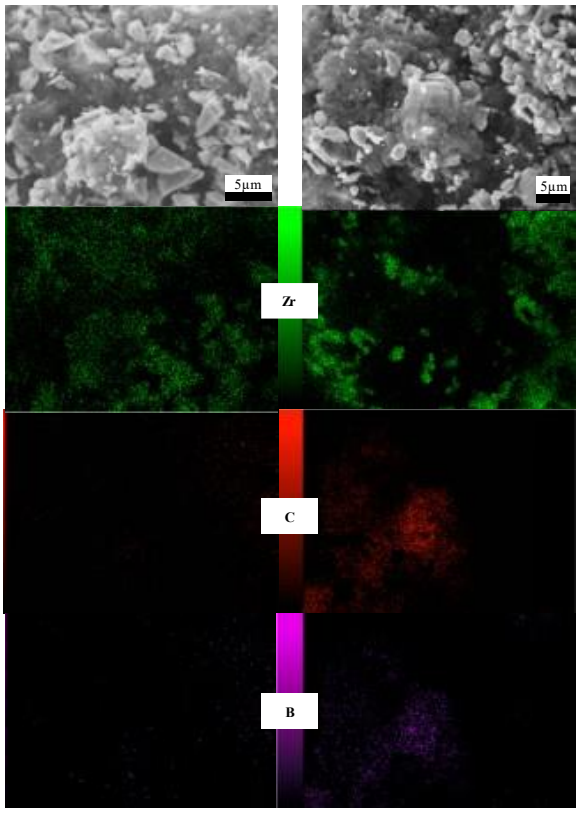

Figure 2. *10wt% MWCNT* ***(left)*** *green and* ***(right)*** *sintered, with elemental maps of zirconium, carbon, and boron.*

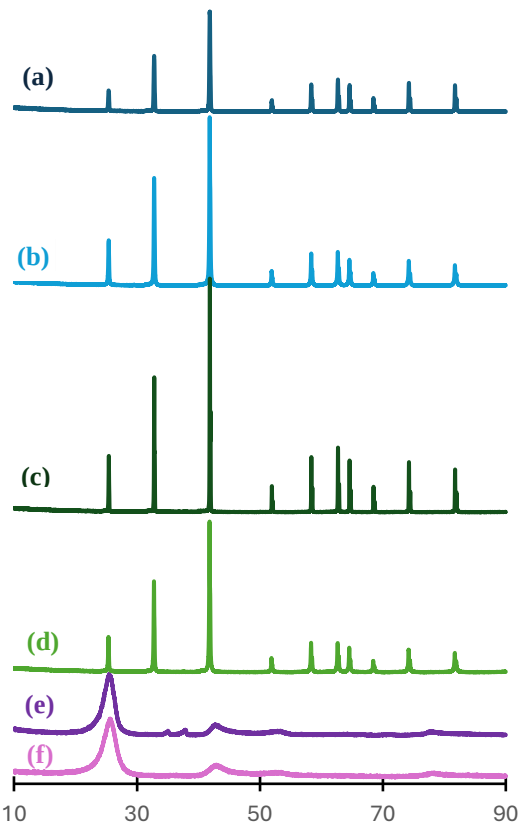

Figure 4. *XRD scans of* ***(a)*** *0wt% MWCNT sintered* ***(b)*** *0wt% MWCNT green* ***(c)*** *10wt% MWCNT sintered* ***(d)*** *10wt% MWCNT green* ***(e)*** *100wt% MWCNT sintered and* ***(f)*** *100wt% MWCNT green*

The 10wt% MWCNTs sample has been the only sample analyzed using XPS thus far. Preliminary investigation shown in Figure 5 indicated no presence of either ZrC or B_4C bonding within the range of zirconium and boron binding energy. Comparison of carbon binding energy is being completed between 0wt%, 10wt%, and 100wt% MWCNTs sintered samples to determine differences that may be present between C-C bonding. Due to the sintering cycle of 2000°C, binding and phase changes within the MWCNTs may be possible and shown within the carbon binding energy once XPS is completed on a sintered 100wt% MWCNTs sample.

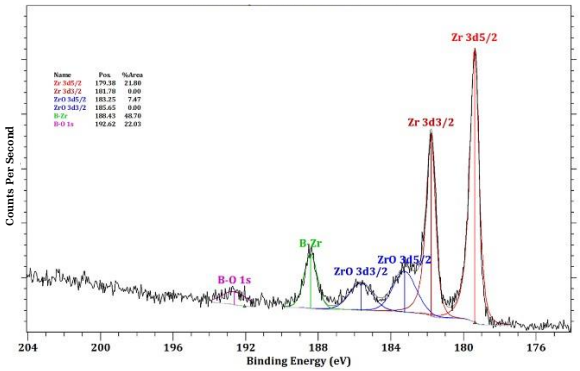

Figure 5*. XPS results of sintered 10wt% MWCNT, in the zirconium and boron binding energy range.*

Conclusion

The role of CNTs in ZrB_2 samples were studied with an increasing MWCNTs weight percentage being created through slip casting. Results from SEM, XRD, and XPS are inconclusive to the potential phase change of MWCNTs when sintered with ZrB_2 at 2000°C. SEM/EDS scans show no strong evidence for boron in the ZrB_2 particles, which makes tracking a potential reaction with the MWCNTs difficult to confirm. Scans completed with XRD indicate no identifiable combination of the nanotubes within 10wt% MWCNT. Additional XPS scans show no change of phase to ZrC or B_4C in a 10wt% MWCNTs sample.

Future Work

Future research should focus on validating the existence of the predicted phases indicated in the ternary phase diagrams through sintering experiments conducting at the corresponding temperatures. Further characterization of the MWCNTs within the ZrB_2 matrix is necessary to fully define their role as a reinforcement mechanism in UHTCs, particularly in use of porous microstructures.

References

[1] D. Sziroczak and H. Smith, “A review of design issues specific to hypersonic flight vehicles,” *Progress in Aerospace Sciences*, vol. 84, pp. 1-28, April 2016, doi: 10.1016/j.paerosci.2016.04.001.

[2] A.B. Peters et al., “Materials design for hypersonics,” *Nature Communications*, Mar. 2024, doi: 10.1038/s41467-024-46753-3.

[3] G. B. Yadhukulakrishnan, “Spark plasma sintering of silicon carbide, multi-walled carbon nanotube and graphene reinforced zirconium diboride ceramic composite,” PhDT, 2012.

[4] A. Raunika, S. Raj, K. Jayakrishna and M. Sultan, 2017. Carbon nanotube: A review on its mechanical properties and application in aerospace industry. IOP Conference Series: Materials Science and Engineering, vol. 270, p. 012027. Available: 10.1088/1757-899x/270/1/012027.

[5] W.W. Wu, M. Estili, G.J. Zhang, and Y. Sakka, “Dispersion and structural evolution of multi-walled carbon nanotubes in ZrB_2 matrix,” *Ceramics International*, vol. 43, pp. 10533-10539, May 2017, doi: 10.1016/j.ceramint.2017.05.111.

[6] W. A. Curtin and B. W. Sheldon, “CNT-reinforced ceramics and metals,” *Materials Today*, vol. 7, no. 11, pp. 44-49, Nov. 2004, doi: 10.1016/S1369-7021(04)00508.

[7] K. F. Chan, M. H. M. Zaid, M. S. Mamat, S. Liza, M. Tanemura, and Y. Yaakob, “Recent Developments in Carbon Nanotubes-Reinforced Ceramic Matrix Composites: A Review on Dispersion and Densification Techniques,” *Crystals*, vol. 11, no. 5, April 2021, doi: 10.3390/crys11959457.

[8] K. L. Niehoff, C. Tallon, and M. Bortner, "Integrating Nanomaterial Enhancements with Multi-scale Zirconium Diboride for Ultra-High Temperature Application," unpublished.

[9] W.M. Guo, L.X. Wu, Y. You, and H.T. Lin, “Three-step reactive hot pressing of B4C-ZrB2 ceramics,” Journal of the European Ceramic Society, vol 36, no. 4, Dec. 2015, doi: 10.1016/j.jeurceramsoc.2015.11.022.

[10] Z. Huang and L. Wu, “Ultrahigh-Temperature Ceramics (UHTCs) Systems,” in Phase Equilibria Diagrams of High Temperature Non-oxide Ceramics. Singapore, Singapore: Springer Nature, 2018, chapter 4, section 12, pp. 116.